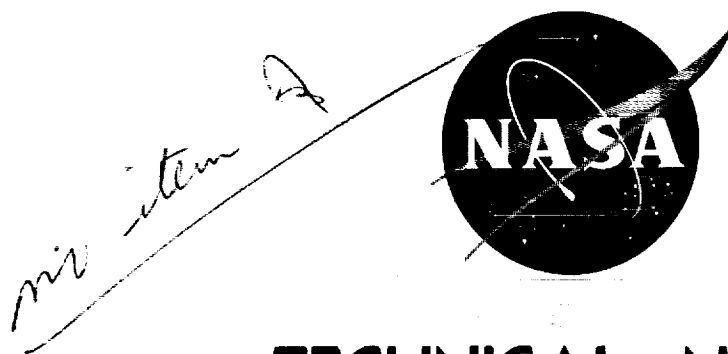


NI Incl

N 62 70595

NASA TN D-21

NASA TN D-21



TECHNICAL NOTE

D-21

NEAR-FIELD AND FAR-FIELD NOISE SURVEYS OF
SOLID-FUEL ROCKET ENGINES FOR A RANGE
OF NOZZLE EXIT PRESSURES

By William H. Mayes, Wade E. Lanford,
and Harvey H. Hubbard

Langley Research Center
Langley Field, Va.

M-11 IC

SEP 4 1959

NATIONAL AERONAUTICS AND SPACE ADMINISTRATION
WASHINGTON

August 1959

G

NATIONAL AERONAUTICS AND SPACE ADMINISTRATION

TECHNICAL NOTE D-21

NEAR-FIELD AND FAR-FIELD NOISE SURVEYS OF
SOLID-FUEL ROCKET ENGINES FOR A RANGE
OF NOZZLE EXIT PRESSURESBy William H. Mayes, Wade E. Lanford,
and Harvey H. HubbardL
2
7
9

SUMMARY

Measurements of near- and far-field noise pressures are presented for a 1,500-pound-thrust engine and for several 5,000-pound-thrust engines for which the nozzle exit pressure was changed systematically in order to study its effects on the noise level and spectra. Near-field surveys indicated that the highest noise pressure occurred at about 20 exit diameters downstream of the nozzle near the transition from supersonic to subsonic flow. The acoustical power radiated from all engines averaged about 0.5 percent of the mechanical power of the exhaust stream, the least noise being radiated by the nozzle having an exit pressure less than atmospheric. The rocket engines of these tests radiate more power per cycle at the lower frequencies than are reported for subsonic jets in other related studies.

INTRODUCTION

The use of solid-fuel rocket engines for assisted-take-off operations of aircraft, and in ground and air launchings of missiles and space vehicles, results in several potentially serious problems due to the intense noise. The near-field noise can result in fatigue failures of structures and the malfunctioning of sensitive equipment located near the rocket engine. The far-field noise can be detrimental to personnel in the launch area and in communities located near launching areas. It is thus desirable to be able to predict the noise environment of rocket engines in the design stage so that adequate protection for structures and equipment as well as personnel may be provided.

Only a limited amount of rocket-engine noise data are presently available for use in such prediction problems. Reference 1 contains the noise radiation pattern of a 1,000-pound-thrust rocket engine of

the type used for thrust augmentation of aircraft at take-off and also contains a few near-field noise measurements for rocket engines ranging from 900 to 5,500 pounds of thrust. Some near- and far-field noise-survey data are contained in references 2 and 3 for both solid- and liquid-fuel rockets ranging in thrusts from 1,000 to 130,000 pounds. Of particular interest is an extensive near-field survey for a 1,000-pound-thrust solid-fuel rocket engine for which the overall noise level contours are given in reference 2.

The data of the present paper are from systematic studies during static firing of a 1,500-pound-thrust engine and of several 5,000-pound-thrust engines for which the jet nozzle exit flow conditions varied widely. Attempts are made to define the near-field noise contours of the 1,500-pound-thrust engine for some of the one-third-octave bands as well as for the overall noise. With regard to the 5,000-pound-thrust engines, an attempt is made to determine the possible effects of changes in the exit flow conditions on both the near and far noise fields. These data provide some information relative to the basic mechanisms of noise generation. They also provide a basis for estimating noise for off-design operating conditions and for engines having higher thrust ratings.

SYMBOLS

A	area, sq ft unless otherwise specified
c	speed of sound, ft/sec
D	nozzle diameter, ft unless otherwise specified
F	thrust, lb
f	mean frequency of band-pass filter, cps
g	acceleration due to gravity, ft/sec ²
M	calculated Mach number
p	pressure, lb/sq ft unless otherwise specified
t	time, sec
V	velocity, ft/sec
W	weight of rocket grain burned, lb
x	axial distance (positive downstream of nozzle), ft

y radial distance, ft

ψ azimuth angle, deg

Subscripts:

a ambient

c chamber

e nozzle exit

t nozzle throat

APPARATUS AND METHODS

Engine Configurations

Six rocket engines were tested during the present survey. The powder grain and accessories of figure 1(a) were used with nozzles A, B, C, D, and E (see fig. 2) in an attempt to obtain some near- and far-field noise data for a range of nozzle exit flow conditions while chamber pressure and throat diameter were kept constant. The smaller powder grain and accessories of figure 1(b) were used with nozzle F to obtain more detailed surveys of both the near- and far-noise fields for fixed nozzle exit flow conditions. Both types of grain were of cruciform cross section having helical inhibitor patterns. The chief constituents of the grain were nitroglycerin and nitrocellulose.

Sectional views of the six test nozzles are shown in figure 2. Nozzle A has eight individual circular exits whereas the other nozzles have single exits. Nozzles B, C, D, and E have the same converging and throat sections and differ only in the length of the conical diverging section. The exit pressure for nozzles A, B, and F is greater than atmospheric, for nozzles C and D is approximately equal to atmospheric, and for nozzle E is less than atmospheric. The engines incorporating the various nozzles are designated engines A, B, C, D, E, and F.

Test Procedure

The tests were made with the engines statically fired on an outdoor thrust stand as shown in the photograph of figure 3. The engine is mounted in a horizontal position with its center line parallel to the ground and approximately 3.5 feet above ground level. A measure of the rocket-engine performance was obtained for each test by recording the

thrust and chamber-pressure time histories. Sample thrust and chamber-pressure data for engine C are shown in figure 4 along with the corresponding time history of sound pressure level measured at an azimuth angle of 90° and a distance of 50 feet. The thrust and the chamber pressure both rise rapidly to some nominal value, remain essentially constant during most of the time history, and then drop rapidly at the end of the time history. The values of thrust and chamber pressure were determined during the steady part of each test and were obtained from records similar to those of figure 4. The sample records shown here are representative of all the records obtained; however, for engine F, which has less thrust, the corresponding quantities would have markedly different values, as can be seen in table I. It should be noted that the values of thrust and chamber pressure given in this table are arithmetic averages of those measured for several rocket-engine firings. The nozzle exit pressure and the exit Mach number (for a ratio of specific heats of 1.22) presented in table I were determined from calculations based on measurements of chamber pressure and a knowledge of the nozzle geometry. The values of velocity given in table I were calculated by the method indicated in the appendix.

The locations of the near- and far-field measurement stations are shown schematically in figure 5 along with a plan view of the test area. All measurements were made in the same horizontal plane as the rocket-engine center line. The near-field stations extend both fore and aft of the nozzle exit plane, and the loci of measuring points are straight lines parallel to the thrust axis and at various radial distances outward from it. For all near-field measurements, the center line of the microphone was oriented perpendicular to the thrust axis of the engine. The far-field measuring stations were located at 15° increments along the circumference of a circle whose radius is 50 feet from the nozzle exit. For engine F, measurements were made at two additional stations at angles of 150° and 165° from the thrust axis at a radius of 25 feet. For the far-field measurement the center line of the microphone was oriented toward the nozzle exit. The reflection of noise caused by the building is believed to have only small effects on the data presented with the possible exception of those far-field data measured toward the front of the engine.

Instrumentation

Sound pressure measurements were made with the use of condenser microphones having a useful frequency range from 5 to 12,000 cps and its associated preamplifier and power supply. The outputs were recorded on two different magnetic tape systems for later playback and analysis.

The far-field data were recorded on an AM recording system having a useful frequency range from 50 to 15,000 cps. Although some near-field

data were obtained for the frequency range from 100 to 10,000 cps, the bulk of the near-field data were recorded on a multichannel FM tape recorder having a useful range from 0 to 2,500 cps, the carrier frequency restricting the upper cutoff limit.

Thrust and chamber pressure were measured with a strain-gage dynamometer and a dynamic pressure gage, respectively, as indicated in figure 3. Recordings of these quantities were made on a multichannel oscillograph to provide time histories similar to that shown in figure 4.

Data Reduction

Analyses were obtained from the tape-recorded sound pressures by use of a one-third-octave-band filtering system and attached pen recorder. A time history was obtained for each microphone station for the overall sound pressure levels, as shown in figure 4, and for each one-third-octave band. In general, the noise levels were essentially constant during the steady part of the test despite small variations in chamber pressure and thrust. The noise levels quoted in this paper are those associated with the steady part of the time history, and no attempt was made to evaluate the levels during the starting and stopping transients.

Inasmuch as more than one firing was necessary to obtain the sound survey for each type of engine and also inasmuch as ambient temperature varied 60° between some firings, one microphone, as indicated in figure 5, was used as a monitoring station to study the repeatability of the tests. The monitor indicated the maximum sound pressure variation to be 3 decibels for engines A and E and to be within 1 decibel for the remaining engines.

RESULTS AND DISCUSSION

In this paper, sound power level and sound pressure level are given in decibels. The sound power level is referred to 10^{-13} watts and the sound pressure level is referred to 0.0002 dyne/cm². The results are presented separately for the near-field and far-field measurements. In the near-field, comparisons are made of sound pressure levels and spectra generated by rocket engines having a range of exit pressures. Near-field sound pressure contours are presented for one engine to give an indication of the nature of the acoustical field surrounding a rocket engine. Polar distributions of the far-field sound pressures along with their frequency spectra are presented for the engines, and a correlation of the acoustical power of an engine to its mechanical power is made.

Near-Field Noise

A sufficient number of measurements were made in the near-field region for engine F to establish contour lines for the overall noise levels and one-third-octave bands up to 2,500 cps. These data are shown in figure 6 as a function of radial and axial distances expressed in terms of nozzle exit diameters. The lines of constant sound pressure level are interpolated between measuring stations and define approximately the near-field region. The shape of the noise contour lines of figure 6(a) which are for a frequency range of 5 to 2,500 cps are such as to suggest an apparent source of noise approximately 20 diameters downstream of the nozzle exit, as in the tests of reference 4 for cold air jets. High-speed motion pictures taken of the flow indicated this region to be near the point where the flow chokes to subsonic velocities. This fact suggests that the subsonic flow region is important with regard to noise generation. The noise contours for the frequency range from 5 to 2,500 cps also indicate that levels in excess of 140 decibels exist over a large region, and it is significant to note that damage to structures and equipment can occur at these noise levels (ref. 5). The data of figure 6(a) are in fair agreement in the region downstream of the nozzle exit with near-field contours available for a 1,000-pound-thrust rocket engine in reference 2.

L
2
7
9

One-third-octave-band sound pressure levels are also presented in figure 6. It is seen from figures 6(b) and 6(c) that the contours for the lower frequencies do not reach a maximum in the distance covered by the test. For the higher frequencies such as shown in figures 6(d), 6(e), and 6(f), some maxima of the contours could be defined, and these maxima occurred nearer the nozzle exit in the axial direction for the higher frequencies. The result suggests that either the apparent sources of the noise in various frequency bands are located at different parts of the jet exhaust stream or that the radiation characteristics of the jet exhaust stream differ for different frequencies. Sufficient data were not obtained to provide contours such as these for all the engines tested, but the limited data did indicate that the same general pattern would exist.

Sound pressure levels were measured in the near-field region for some of the larger rockets tested, and these are shown in figures 7 and 8. The data of figure 7 for engines B, C, and E were measured at a given radial distance of 3 feet from the thrust axis. Sound pressure levels are shown as a function of distance as measured from the minimum throat section, which as indicated in figure 2 is at the same relative location for each engine. It will be noted that the sound pressure levels increase generally in the downstream direction. Part of this increase is, of course, due to the fact that the microphone is closer to the boundary of the exhaust jet. The data show that the pressure levels at a given distance in the near-field are, in general, lower for

engine C, which has an exit pressure approximately equal to atmospheric pressure. The fact that the sound pressure levels for engine E are only slightly higher than comparable values for engine C indicates that there is only a small penalty for overexpansion at the nozzle exit.

Better correlation of the data from the three engines is obtained when the distance is nondimensionalized as in figure 8. In this figure, sound pressure level is plotted as a function of $\frac{x}{D_e}$ for $\frac{y}{D_e} = 3$. As a result, the data come close together and the scatter is minimized with the exception of the region close to the nozzle exit plane. For these engines, the region of measurements close to the nozzle exit is apparently influenced by the exit flow conditions to a greater extent than regions either upstream or downstream from the nozzle. Good agreement in the region $\frac{x}{D_e} = 30$ and $\frac{y}{D_e} = 30$ downstream from the nozzle may be fortuitous and may result from the fact that the contours of the sound pressure levels are essentially radial lines extending from the nozzle as indicated in figure 6(a). This has the effect of making the sound pressure levels nearly independent of distance and primarily a function of direction relative to the nozzle.

Also shown in figure 8 are some free-field data from reference 3 for four configurations of rocket engines having 100,000 and 130,000 pounds of thrust. These data are for rather extreme test conditions and are noted to have a scatter approximately equal to that of the present tests. The sound pressure levels are somewhat higher than the levels of the present tests, possibly due, in part, to the wider frequency range of the measuring equipment used.

Sample spectra obtained in the near field at locations 2.5 diameters upstream and 11.5 diameters downstream of the nozzle for engine C are given in figure 9. Data have been adjusted to unit band width for purposes of comparison. Both spectra are seen to have broad maxima near 1,000 cps. It can also be seen that the spectrum for the downstream location has a relatively larger amount of low-frequency noise and relatively less high-frequency noise than the spectrum for the upstream location. For points far downstream, there is a tendency for the spectra to peak at frequencies well below 1,000 cps, as suggested by the contour plots of figure 6. Spectra for the other near-field locations of figure 8 for engine C were similar in shape to those illustrated in figure 9. The spectra for engines B, D, and E were also similar in shape to those of engine C and differed in only minor respects. The spectra for engine A differed from all others because of the presence of a strong component having a frequency of about 400 cps, as illustrated in figure 10(a).

Figure 10 includes time histories of the near-field noise from engine A and engine C for comparison. The data for engine C were typical

of the records obtained for engines having predominantly random-noise spectra. The data for engine A, on the other hand, included a strong discrete frequency component which is evident in the time-history trace of the noise pressure. The customary random-noise pressure variation due to jet mixing appears to be superposed on a discrete frequency component. The origin of the discrete frequency noise is not known, although it may be associated with a cavity resonance of the chamber or an exit flow instability. It was noted that the discrete frequency noise component was relatively less important at field points downstream of the nozzle where the random noise levels were highest and relatively more important upstream of the nozzle.

Far-Field Noise

Measurements were made for rocket engines A, B, C, D, E, and F in the far-field region at stations as defined by figure 5. One-third-octave-band sound pressure levels in the range from 100 to 10,000 cps are given in table II, and the main results are illustrated by the curves of figures 11 to 14.

Overall sound pressure levels and levels in the one-third-octave bands having mean frequencies of 250 and 2,500 cps are plotted as a function of azimuth angle for several engines in figure 11. The nozzle exit location is at the origin and the flow is in the direction of the 0° azimuth line. The one-third-octave band with a mean frequency of 250 cps has its maximum values at azimuth angles in the vicinity of 30° to 45° from the thrust axis in the rear of the engine. On the other hand, the one-third-octave band having a mean frequency at 2,500 cps is noted to be somewhat less directional, the maximum levels occurring at azimuth angles in the range from 75° to 120° . From figure 11 and also from the data of table II, it can be seen that the lower frequency components tend to be stronger at the smaller azimuth angles whereas the higher frequency components are stronger at the larger azimuth angles. The maximum overall noise levels for all engines occur at azimuth angles in the vicinity of 30° to 45° . Engine F, which has a lower thrust rating than the other engines, also usually generates lower noise levels. It can also be seen that, in general, for the engines of comparable thrust, the lower noise levels are associated with engine E.

The sound power level for each one-third-octave band was obtained from the data of table II and by the use of an integration method outlined in reference 6. For the calculations, it was assumed that the acoustical power was radiated in a hemisphere and that there was radial symmetry of the noise pressure field. The results are shown in figure 12 in the form of power spectrum level in the frequency range from 100 to 10,000 cps. The curves are, in general, double-peaked; the highest peak

occurs at frequencies of 200 to 500 cps and another lower peak occurs at frequencies of 2,000 to 4,000 cps. The small dips in the curves in the vicinity of 1,000 cps are believed to result from the fact that the signal reflected from the ground tends to cancel the direct signal in this frequency range for the geometry of the test setup. (See ref. 7.) The curve for engine A has an additional peak at about a frequency of 400 cps because of the presence of a discrete noise component, as noted previously in figure 10(a).

L The data of figure 12 have been normalized in the same manner as in
2 figure 45B of reference 3 and the results are shown in figure 13. This
7 presentation involves the use of the calculated speed of sound in the
9 gas flow at the nozzle exit and the exit diameter as the scaling parameters. The diameter for engine A is based on the total sum of the exit areas of the individual nozzles for engine A. The short-dash curve, which represents a fairing through the data of reference 3, is included for comparison. The data of the present tests are seen to scatter about this curve and are, in general, in agreement with it. Thus it appears that this is a useful method of generalizing the spectral characteristics of noise for rocket engines of widely different sizes and nozzle exit conditions. The range in which the present data fall below the curve from reference 3 corresponds to frequencies near 1,000 cps where low values were also noted in the curves of figure 12.

The present tests provided more data at the low values of the dimensionless frequency parameter than did the tests of reference 3, and in so doing indicated a very broad peak of this spectrum. Comparable data for subsonic jets also have a characteristic spectrum, as shown in references 6 and 8, and the long-dash curve, which is estimated for turbojet engines from the data of reference 6, is included in figure 13 for comparison. (For engine operation near choking pressure ratios of the nozzle, the exit velocity as used in ref. 6 is approximately equal to the speed of sound in the exhaust.) The maximum of this latter curve is seen to be more sharply defined, however, and occurs at a value of the nondimensional frequency parameter between 0.1 and 0.2. A comparison of these data indicates that supersonic jets tend to radiate more power per cycle at the lower frequencies than do subsonic jets.

The total acoustical power calculated from the data of figure 12 for five rocket engines is shown by the solid test points in figure 14 as a function of the mechanical power in the jet exhaust stream. The mechanical power was calculated as the product of the thrust and exit velocity (given in table I). Also shown in the figure are data from references 1 and 6 for rocket engines in the thrust range from 1,000 to 130,000 pounds. A dashed line indicating 0.5-percent acoustical-mechanical efficiency is drawn in to aid in the comparison of the data. The data are seen to fall about this line, particularly at the high values

of power. The data from the present tests showed that approximately 0.3 to 0.8 percent of the total jet stream power was radiated as noise, the least amount being associated with engine E and the largest amount with engine A. The results of figure 14 suggest that a rough correlation exists between the radiated acoustical power and the mechanical power in the jet exhaust stream of a rocket engine, and this correlation does not vary noticeably as engine power varies.

CONCLUSIONS

Near- and far-field noise surveys for six different rocket engines in the 1,500- and 5,000-pound thrust range indicated the following conclusions:

1. The apparent sources of the noise were located 20 or more diameters downstream of the nozzle exit in the region of subsonic flow.
2. The lowest near-field noise pressures measured at a given radial distance were from engines having exit pressures approximately equal to atmospheric.
3. Approximately 0.3 to 0.8 percent of the total jet stream power was radiated as noise, the least amount being associated with an engine having overexpanded nozzle exit flow conditions.
4. The rocket engines of these tests radiate more power per cycle at the lower frequencies than are reported for subsonic jets in other related studies.

Langley Research Center,
National Aeronautics and Space Administration,
Langley Field, Va., April 16, 1959.

L
2
7
9

APPENDIX

METHOD USED FOR CALCULATIONS OF EXIT VELOCITY

If the instantaneous rate of expulsion of mass flow from the nozzle exit of a rocket is known, the exit velocity V_e can be calculated by solving the following equation, which is given in reference 9:

$$F = \left(\frac{\dot{W}}{g}\right)V_e + (p_e - p_a)A_e$$

Solving for the instantaneous exit velocity yields

$$V_e = \frac{g[F - (p_e - p_a)A_e]}{\dot{W}} \quad (1)$$

However, since there is no way of directly measuring \dot{W} , which is the weight flow rate of propellant from the nozzle exit, the integrals of all the variables in equation (1) can be evaluated for the burning time of the rocket. Thus, an arithmetic average of V_e may be obtained by use of the following equation:

$$V_e = \frac{g \int_0^t [F - (p_e - p_a)A_e] dt}{W} \quad (2)$$

For the value of W used in equation (2), 7 percent sliver loss or unburned grain was assumed.

Mach number at the exit is constant during the time that the critical pressure for expansion to ambient conditions is exceeded in the combustion chamber of the rocket engine. This pressure is exceeded for very nearly the entire burning period of the rocket engine. During the period that the critical pressure is exceeded in the rocket chamber, Mach number is essentially constant and exit velocity can vary only because of variations in the stagnation temperature of the propulsive gases at particular points in their flow. Inasmuch as the variations in stagnation temperatures are very small, it is assumed that V_e , which is the arithmetic mean for the entire burning time of the rocket motor, is very close to the value of V_e at any particular time during the burning of the rocket.

REFERENCES

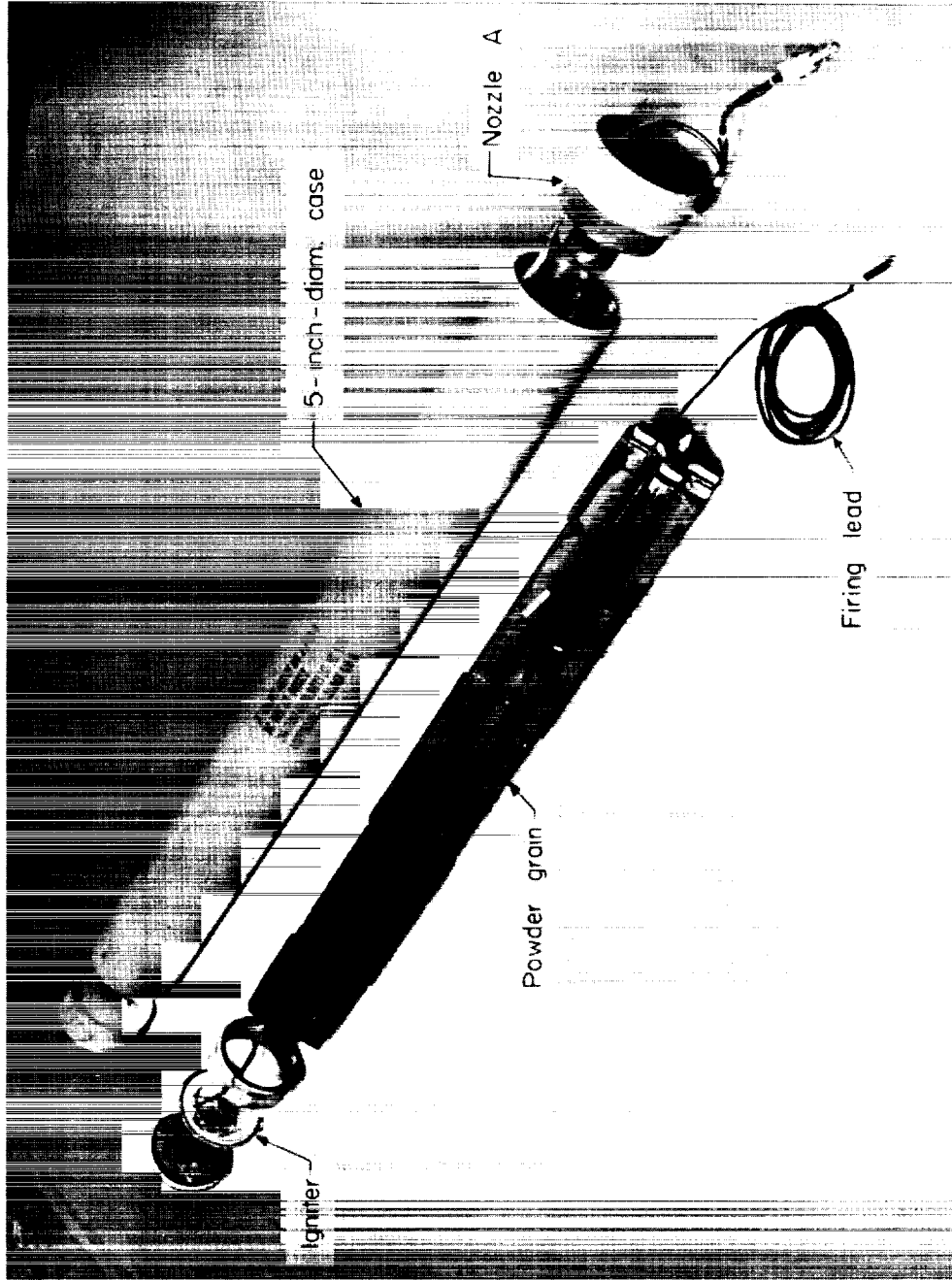
1. Lassiter, Leslie W., and Heitkotter, Robert H.: Some Measurements of Noise From Three Solid-Fuel Rocket Engines. NACA TN 3316, 1954.
2. Humphrey, Allan J.: Rocket Noise Environments. Shock and Vibration Bulletin No. 25, Pt. II, Dept. of Defense, Dec. 1957, pp. 10-17.
3. Cole, J. N., Von Gierke, H. E., et al.: Noise Radiation From Fourteen Types of Rockets in the 1,000 to 130,000 Pounds Thrust Range. WADC Tech. Rep. 57-354, AD 130794, U. S. Air Force, Dec. 1957.
4. Mull, Harold R., and Erickson, John C., Jr.: Survey of the Acoustic Near Field of Three Nozzles at a Pressure Ratio of 30. NACA TN 3978, 1957.
5. Hess, Robert W., Fralich, Robert W., and Hubbard, Harvey H.: Studies of Structural Failure Due to Acoustic Loading. NACA TN 4050, 1957.
6. Von Gierke, Henning E.: Aircraft Noise Sources. Handbook of Noise Control, ch. 33, Cyril M. Harris, ed., McGraw-Hill Book Co., Inc., 1957, pp. 33-1 - 33-65.
7. Franken, Peter A.: A Theoretical Analysis of the Field of a Random Noise Source Above an Infinite Plane. NACA TN 3557, 1955.
8. Mawardi, Osman K., and Dyer, Ira: On Noise of Aerodynamic Origin. Jour. Acous. Soc. of America, vol. 25, no. 3, May 1953, pp. 389-395.
9. Sutton, George P.: Rocket Propulsion Elements. Second ed., John Wiley & Sons, Inc., 1957, p. 88.

TABLE I.- PHYSICAL CHARACTERISTICS AND OPERATING
CONDITIONS OF VARIOUS ROCKET ENGINES

Rocket engine	A_t , sq in.	A_e , sq in.	F , lb	P_c , lb/sq in. abs	P_e , lb/sq in. abs	V_e , ft/sec	M_e
A	2.45	9.82	6,120	1,541	65.0	7,260	2.65
B	2.45	12.27	7,400	2,021	61.3	7,495	2.82
C	2.45	27.98	6,730	1,728	17.3	8,065	3.43
D	2.45	38.04	8,125	2,160	14.3	8,355	3.67
E	2.45	64.54	7,150	1,918	6.4	8,760	4.07
F	1.77	6.54	1,650	794	37.0	6,600	2.59

TABLE II.- ONE-THIRD-OCTAVE-BAND SOUND PRESSURE LEVELS AT A DISTANCE
OF 50 FEET FOR VARIOUS ROCKET ENGINES

Azimuth angle, ψ, deg	Sound pressure level, db, for -																				
	100 cps	125 cps	160 cps	200 cps	250 cps	320 cps	400 cps	500 cps	640 cps	800 cps	1,000 cps	1,250 cps	1,600 cps	2,000 cps	2,500 cps	3,200 cps	4,000 cps	5,000 cps	6,400 cps	8,000 cps	10,000 cps
Engine A																					
15	124	126	124	124	121	121	134	123	121	129	123	126	124	121	121	119	119	119	119	118	116
30	127	133	136	136	136	135	138	131	129	127	125	126	128	128	127	126	126	125	123	122	120
45	129	136	138	141	141	141	140	138	134	130	130	132	132	130	130	129	129	128	128	128	127
60	122	129	126	129	129	130	136	126	133	134	132	133	133	133	130	128	129	128	128	125	125
75	119	120	121	121	122	124	131	119	126	129	129	132	133	133	130	128	127	127	125	126	126
90	112	114	115	117	115	117	127	109	119	125	127	127	127	128	131	130	129	129	130	127	119
105	110	115	114	115	115	117	129	109	121	125	127	129	127	126	129	130	128	129	130	127	118
120	112	115	116	117	115	118	131	125	124	127	127	127	128	129	131	130	129	128	128	124	115
135	112	115	114	117	115	117	127	124	125	127	128	128	125	127	128	128	128	127	126	123	114
Engine B																					
15	130	132	133	130	128	128	129	126	124	123	122	118	123	121	121	122	124	122	122	122	121
30	135	136	135	139	137	137	136	132	128	126	125	128	127	126	125	124	127	127	125	125	126
45	128	135	136	136	137	138	138	136	134	130	128	128	130	131	128	126	126	126	127	126	124
60	119	121	123	125	125	127	130	130	127	126	124	128	129	127	124	122	124	124	122	121	123
75	111	116	115	116	117	119	122	122	122	123	124	125	126	126	125	123	122	123	124	123	121
90	119	125	122	122	122	121	122	121	119	118	118	121	123	128	130	131	128	127	127	123	114
105	114	119	115	120	121	120	124	124	124	121	122	123	123	125	130	132	130	129	126	124	115
120	110	112	113	113	111	113	114	114	114	114	117	118	121	123	125	125	124	122	122	120	114
135	112	113	113	113	111	112	116	115	118	120	121	120	120	121	123	124	124	122	121	120	114
Engine C																					
15	122	126	126	126	125	120	122	118	118	116	113	111	111	111	110	109	109	111	110	109	108
30	133	138	138	139	138	138	137	134	133	129	128	125	126	128	127	124	127	127	127	126	126
45	129	135	137	141	142	142	141	138	138	134	132	130	131	131	131	129	131	129	130	131	131
60	126	128	128	127	128	132	134	124	131	133	133	133	134	134	132	128	129	127	127	126	125
75	118	123	124	127	127	128	130	130	129	127	127	130	132	134	133	130	129	129	129	129	128
90	114	118	118	119	117	118	121	110	120	121	123	126	128	129	128	127	126	126	126	125	125
105	111	113	114	115	114	115	116	105	116	120	123	125	126	113	129	131	127	127	128	125	118
120	112	114	114	116	115	116	118	108	118	120	123	124	124	125	126	127	125	124	125	122	114
135	113	119	117	119	119	120	131	127	128	125	121	120	125	124	125	123	122	122	122	122	122
Engine D																					
45	131	134	136	137	137	138	136	127	135	134	134	134	135	135	134	130	128	129	129	129	127
90	118	119	123	120	118	118	122	112	123	125	127	128	131	130	129	127	126	126	126	126	126
105	110	112	115	111	114	114	116	106	118	119	123	126	126	126	127	129	126	126	128	125	118
120	107	111	111	112	111	114	115	105	114	117	121	122	123	123	125	126	125	125	128	125	115
Engine E																					
15	130	130	131	129	124	124	124	119	121	122	122	120	121	120	119	119	119	120	120	119	117
30	127	129	130	130	128	128	126	123	121	122	122	123	122	121	119	118	118	119	119	118	118
45	129	133	134	135	134	134	133	124	132	131	132	133	127	122	119	128	126	127	126	126	125
60	120	121	123	127	126	127	131	131	130	128	126	131	130	130	127	124	125	126	125	125	125
75	123	123	122	123	123	124	126	116	124	126	127	131	133	131	129	127	128	125	124	124	125
90	108	110	112	112	112	113	115	114	115	115	118	120	122	124	125	125	124	121	121	120	114
105	118	117	119	121	118	122	124	126	126	126	127	129	128	131	134	134	132	129	130	127	118
120	112	115	114	115	112	115	116	114	115	118	120	120	122	124	126	126	125	124	124	120	114
135	113	114	114	114	115	117	118	117	120	121	123	124	124	126	128	127	125	127	128	125	118
Engine F																					
15	119	121	117	118	118	121	120	118	119	119	117	116	118	120	119	118	118	119	120	118	116
30	124	128	128	130	130	131	130	126	125	123	118	120	123	125	123	121	122	122	122	120	118
45	120	127	128	130	128	130	133	133	133	130	128	124	123	125	125	123	125	125	125	123	123
60	112	114	116	117	117	123	125	124	123	119	119	125	127	125	122	118	123	125	119	118	120
75	114	114	114	113	117	118	120	120	122	121	121	122	123	125	125	125	128	127	124	122	123
90	104	109	109	110	109	110	112	111	112	115	118	120	123	125	124	121	122	122	122	121	121
105	101	102	105	106	105	106	109	107	110	114	118	121	123	123	124	128	124	124	125	124	115
120	109	117	115	116	111	113	114	115	117	119	121	119	121	125	127	128	126	123	124	121	112
135	100	106	104	111	111	113	114	114	116	117	117	118	120	124	126	125	120	121	120	116	108



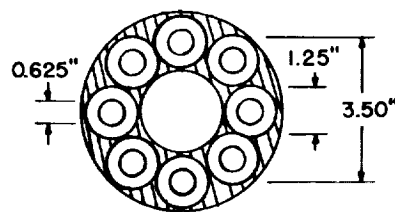
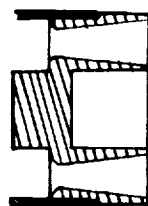
(a) Powder grain and accessories used with nozzles A, B, C, D, and E. L-76086.1

Figure 1.- Photographs of unassembled rocket engines.

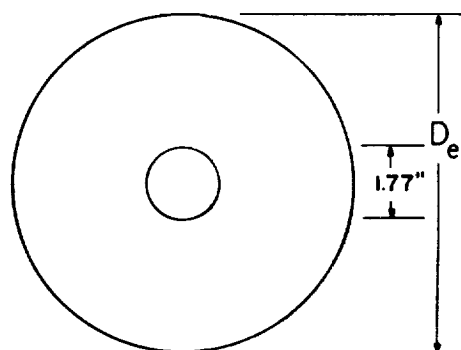
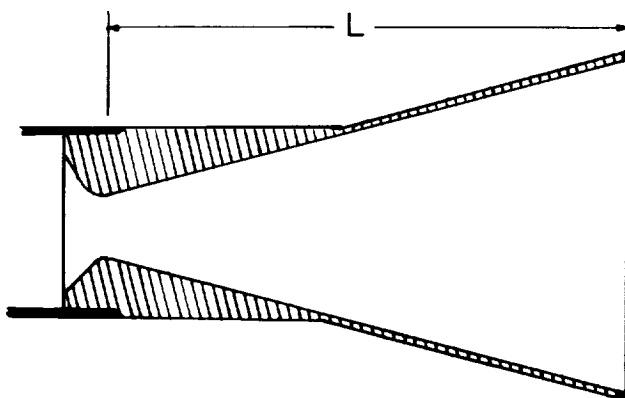


(b) Powder grain and accessories used with nozzle F. L-58-275a.1

Figure 1.- Concluded.

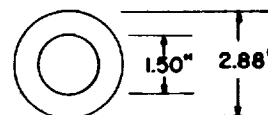
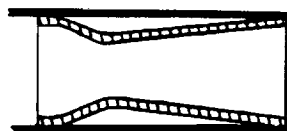


Nozzle A



Nozzle	L, in.	D _e , in.
B	4.09	3.95
C	7.85	5.97
D	9.70	6.96
E	13.63	9.07

Nozzles B, C, D, and E



Nozzle F

Figure 2.- Sectional views of the six test nozzles used in rocket-engine noise survey.

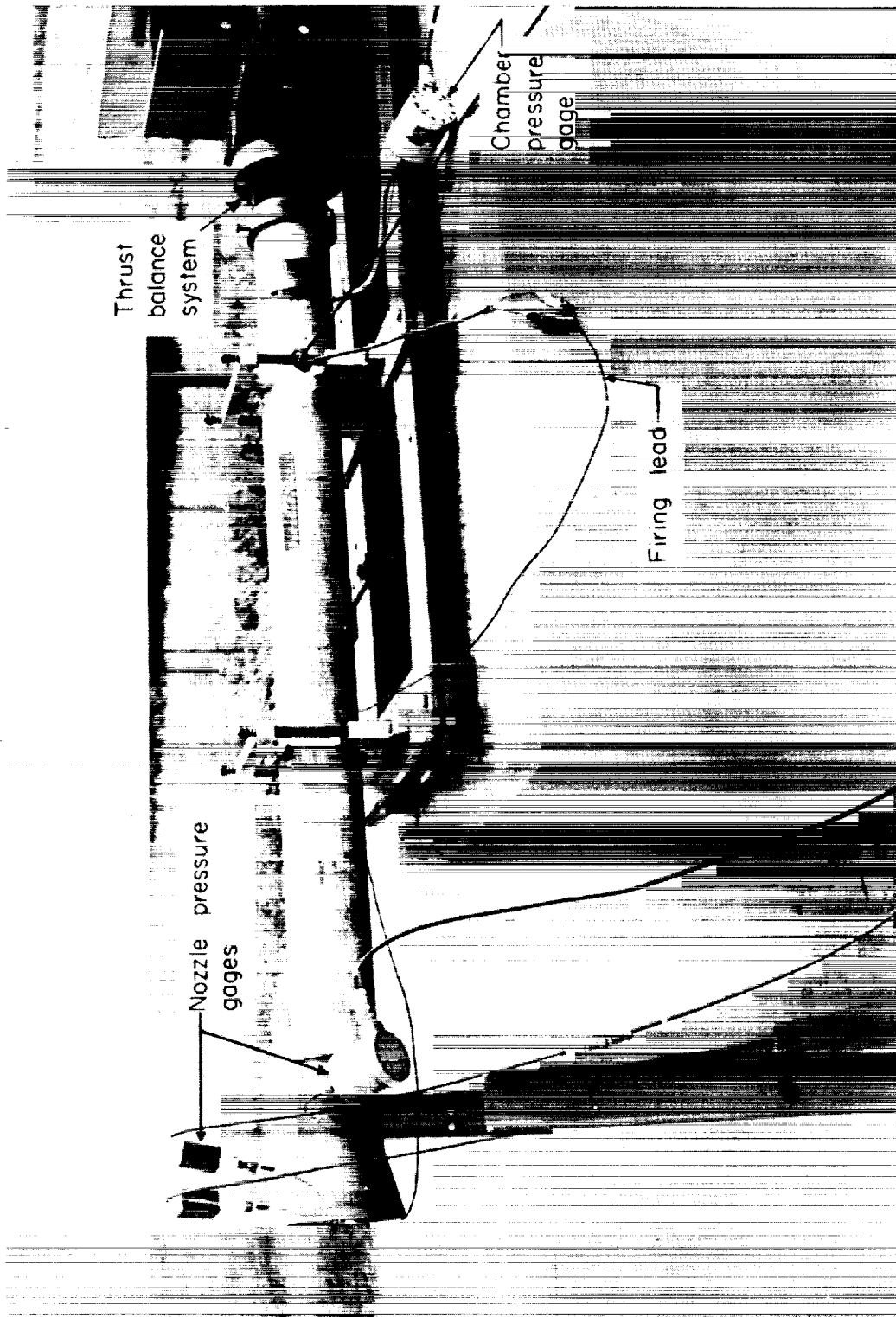


Figure 3.- Photograph of rocket engine D in firing position on outdoor thrust stand.

L-57-3064.1

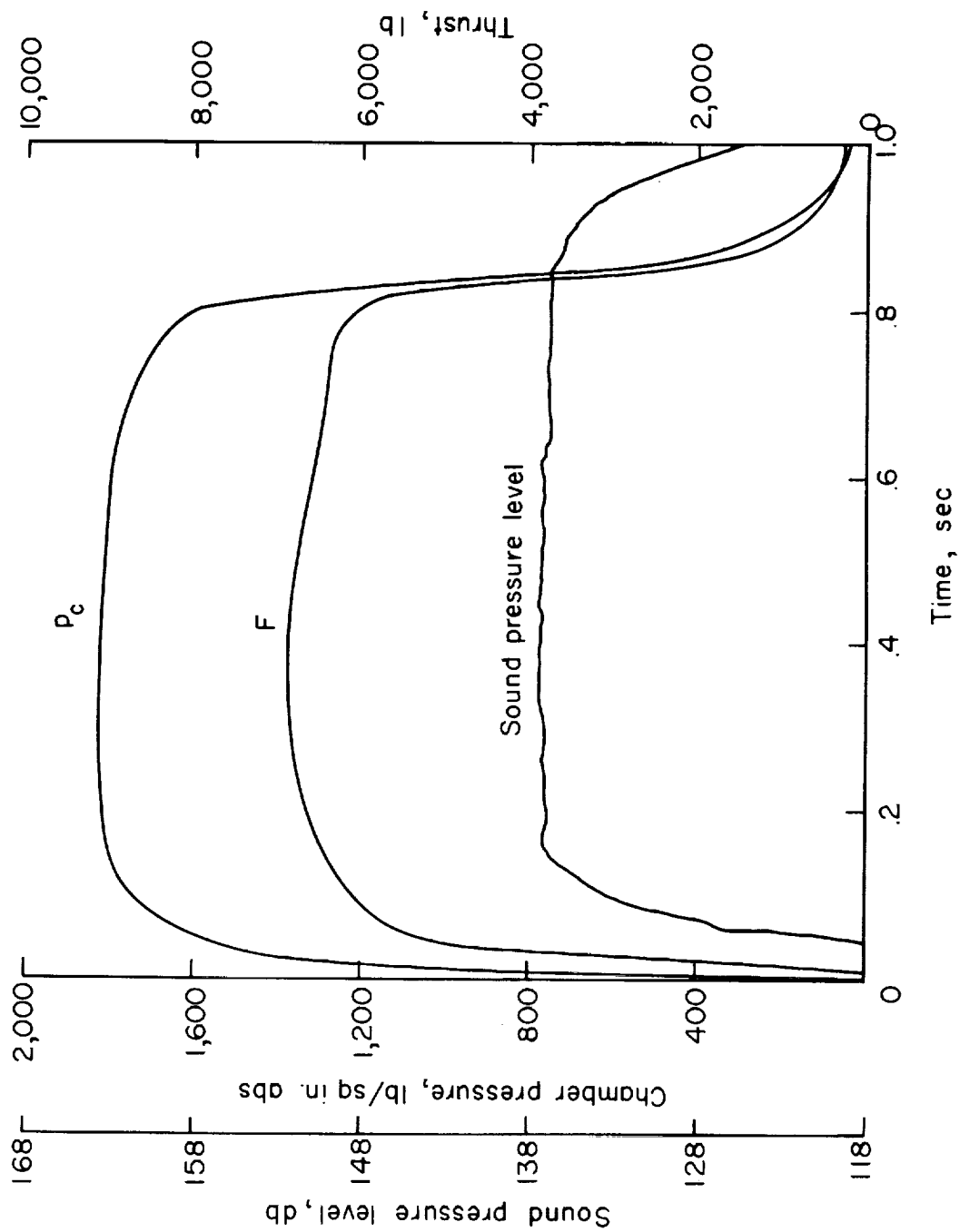


Figure 4.- Time history of chamber pressure, thrust, and sound pressure level for rocket engine C. Sound pressure applicable for a station at a radius of 50 feet and $\psi = 90^\circ$.

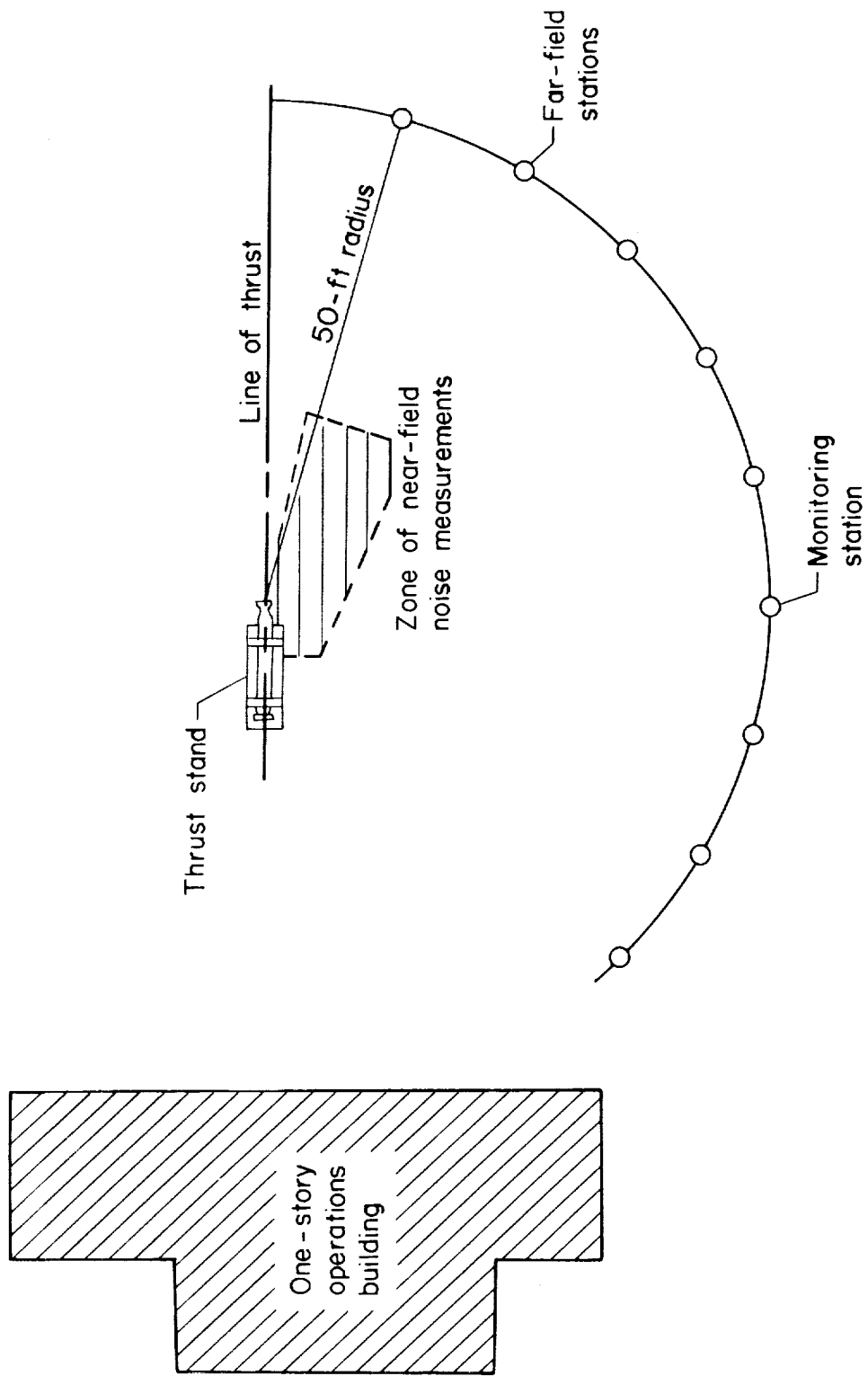
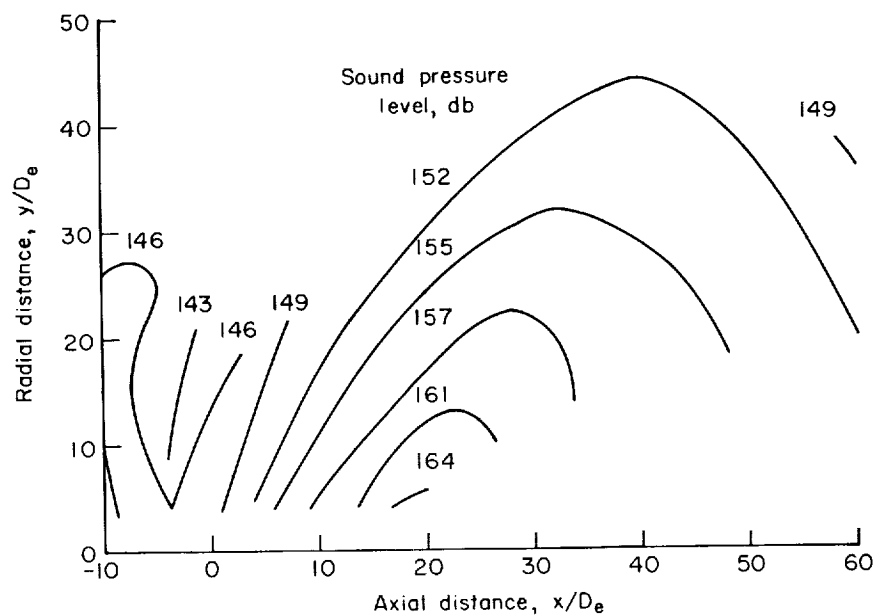
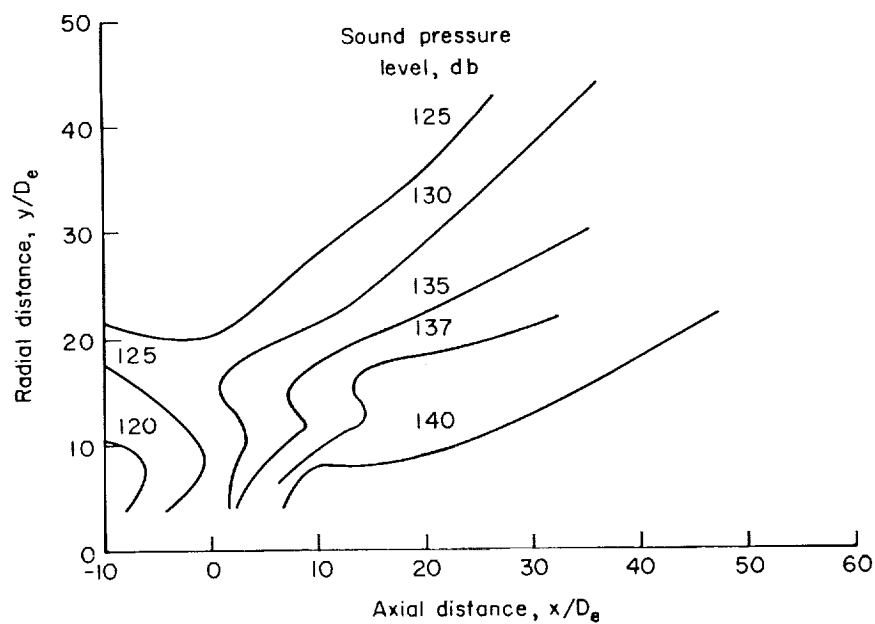


Figure 5.- Plan view sketch of test area, showing measurement stations for rocket-engine noise surveys.

L-279

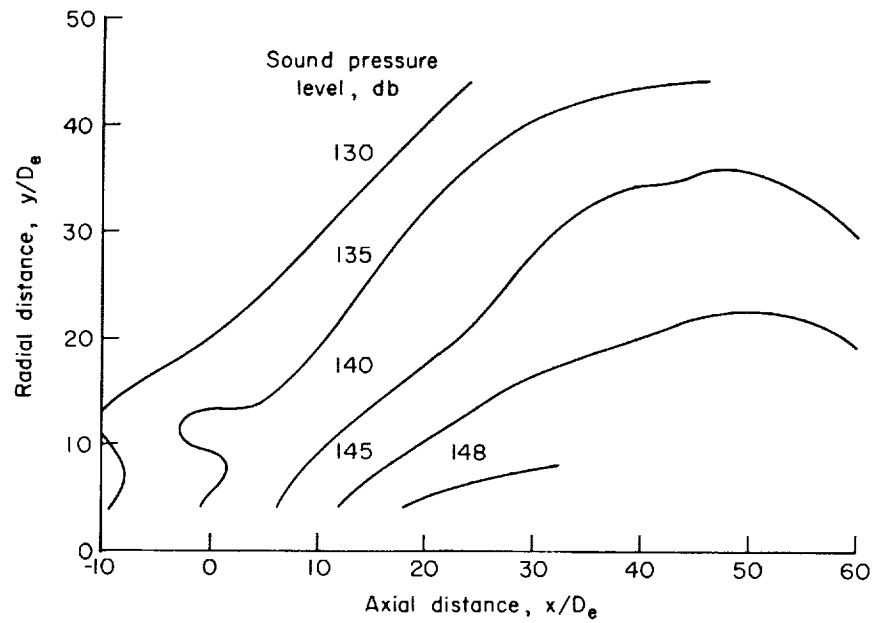


(a) Frequency band, 5 to 2,500 cps.

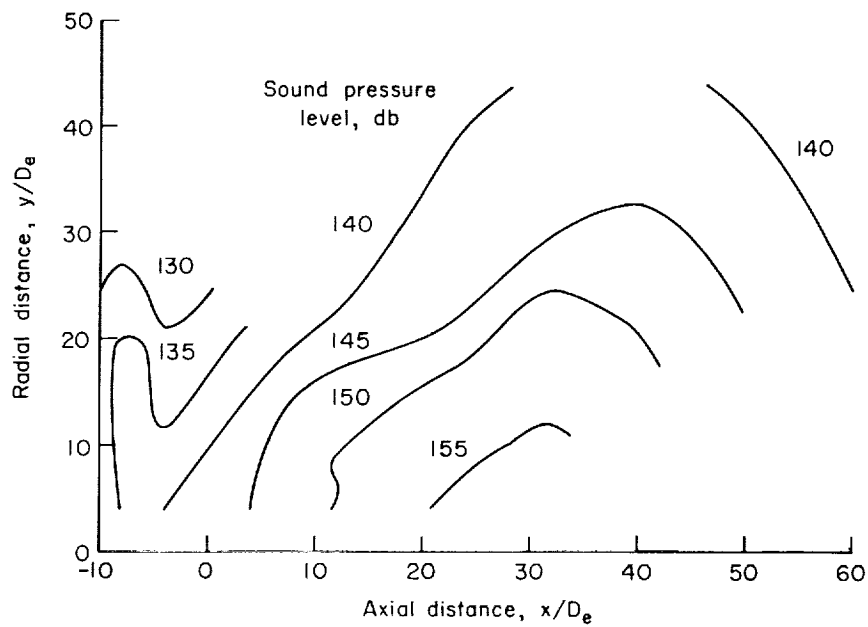


(b) Frequency band, 178 to 224 cps.

Figure 6.- Contours of near-field sound pressure level for rocket engine F.



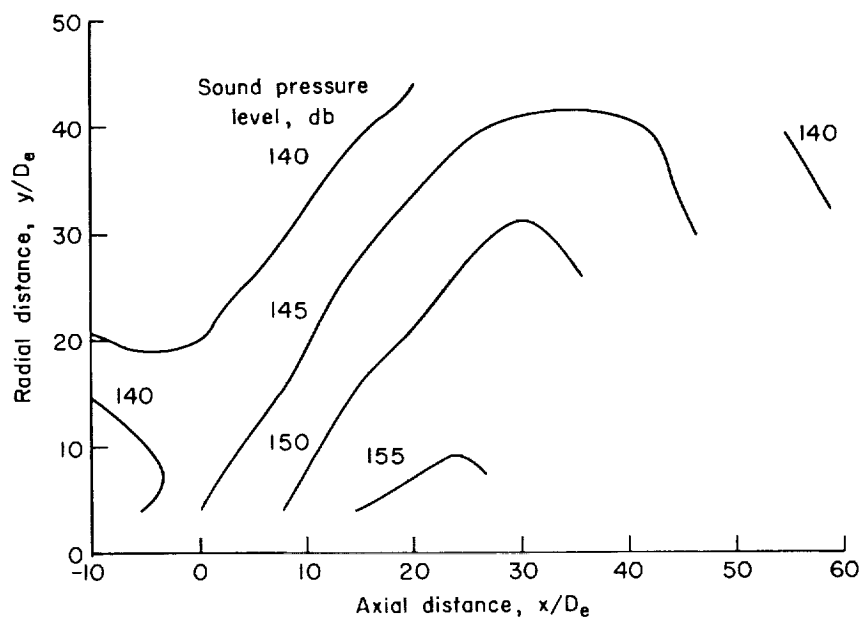
(c) Frequency band, 448 to 566 cps.



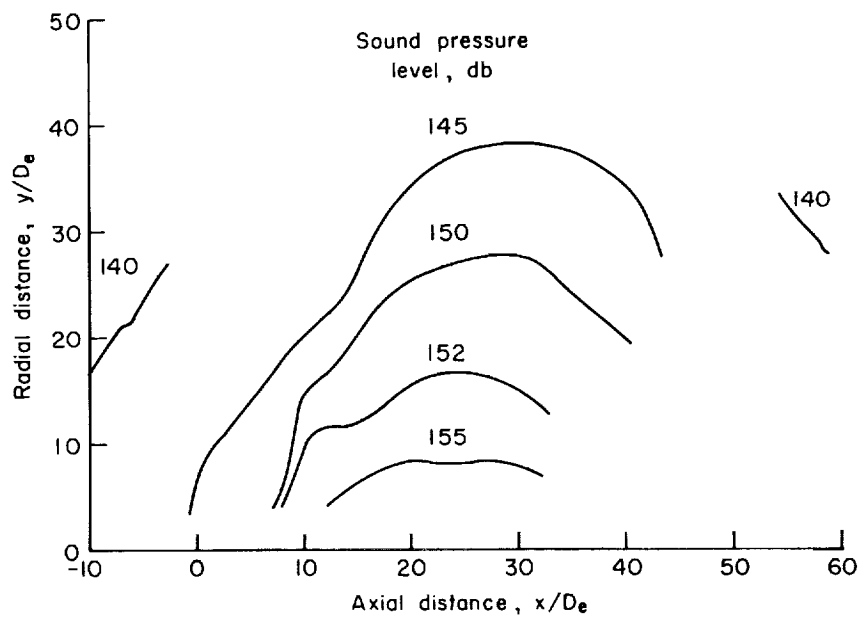
(d) Frequency band, 896 to 1,132 cps.

Figure 6.- Continued.

L-279



(e) Frequency band, 1,410 to 1,780 cps.



(f) Frequency band, 1,782 to 2,264 cps.

Figure 6.- Concluded.

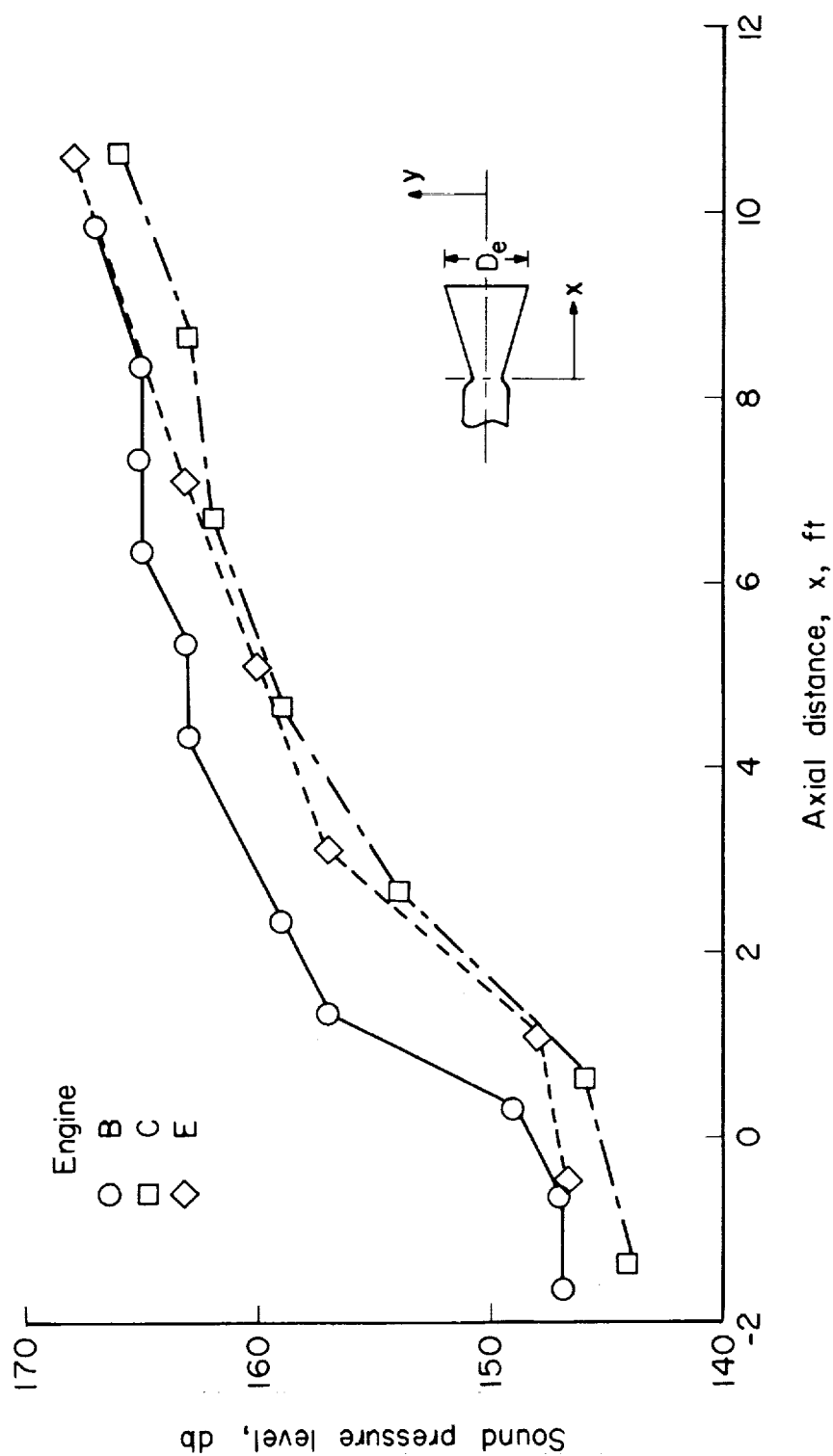


Figure 7.- Sound pressure levels in the frequency range from 5 to 2,500 cps as a function of axial distance in feet for three rocket engines. $y = 3$ feet.

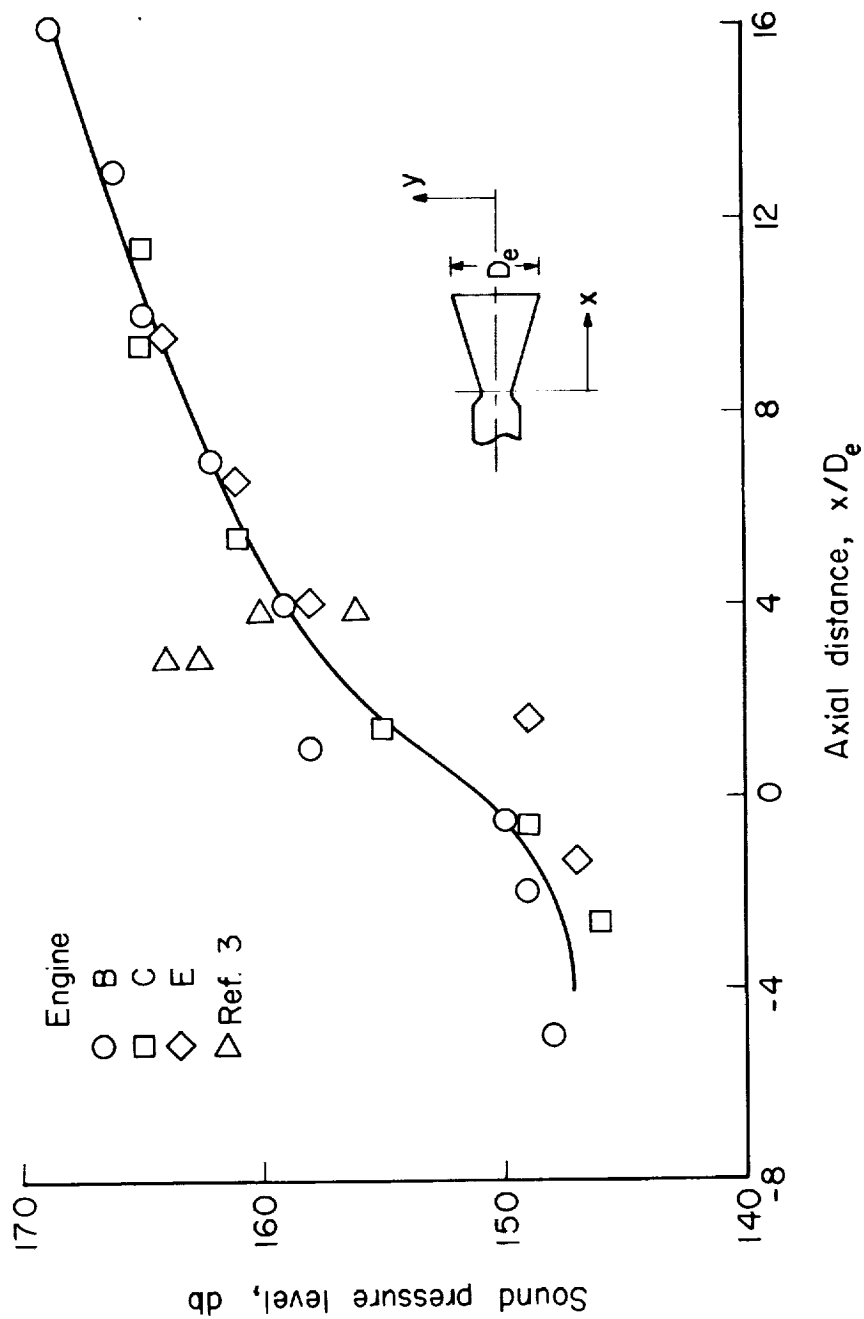


Figure 8.- Sound pressure level in the frequency range from 5 to 2,500 cps as a function of axial distance in diameters for several rocket engines. $\frac{y}{D_e} = 3$.

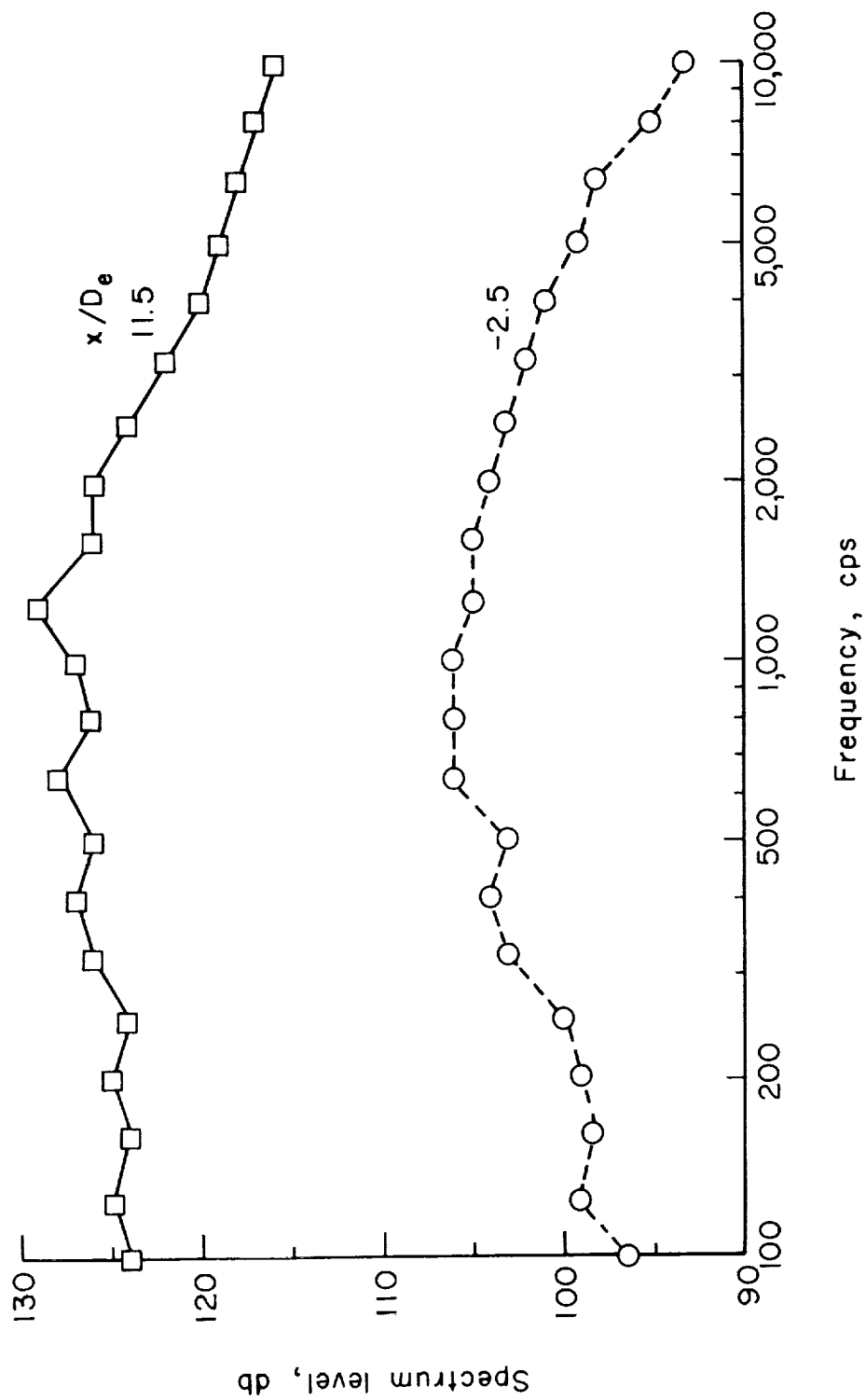
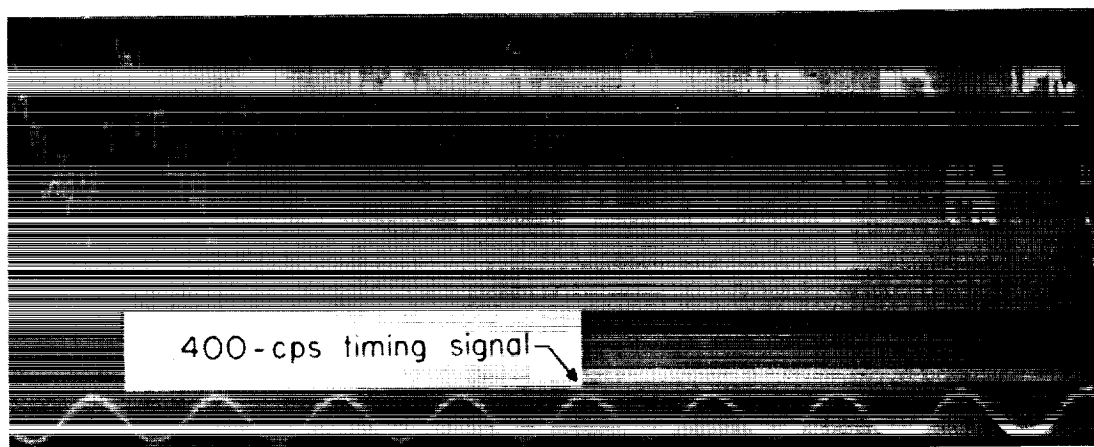
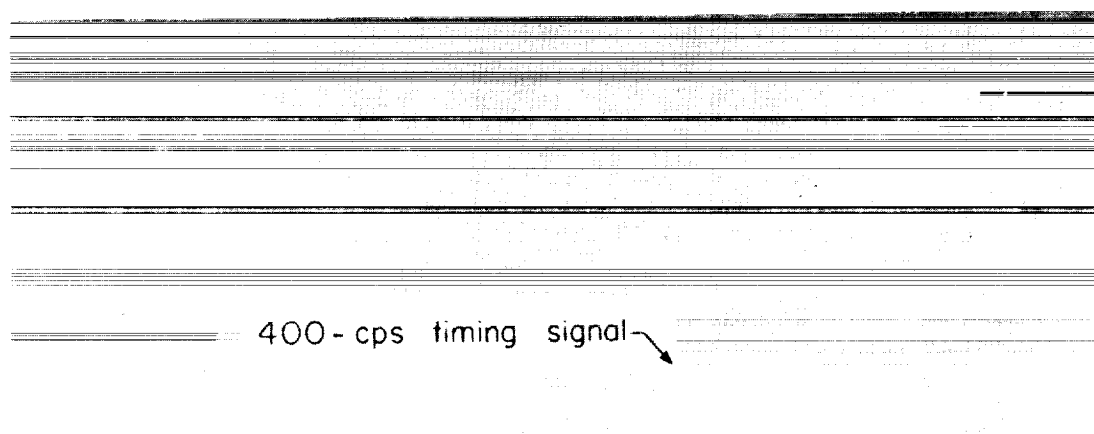


Figure 9.- Sample near-field spectra at locations both upstream and downstream of the nozzle for rocket engine C. $\frac{V}{D_e} = 3$.



(a) Near-field noise from engine A. Overall sound pressure level, 153 decibels.



(b) Near-field noise from engine C. Overall sound pressure level, 150 decibels.

Figure 10.- Time histories of noise from rocket engines A and C measured at a radial distance of 1 foot and an axial distance upstream of 2 feet.

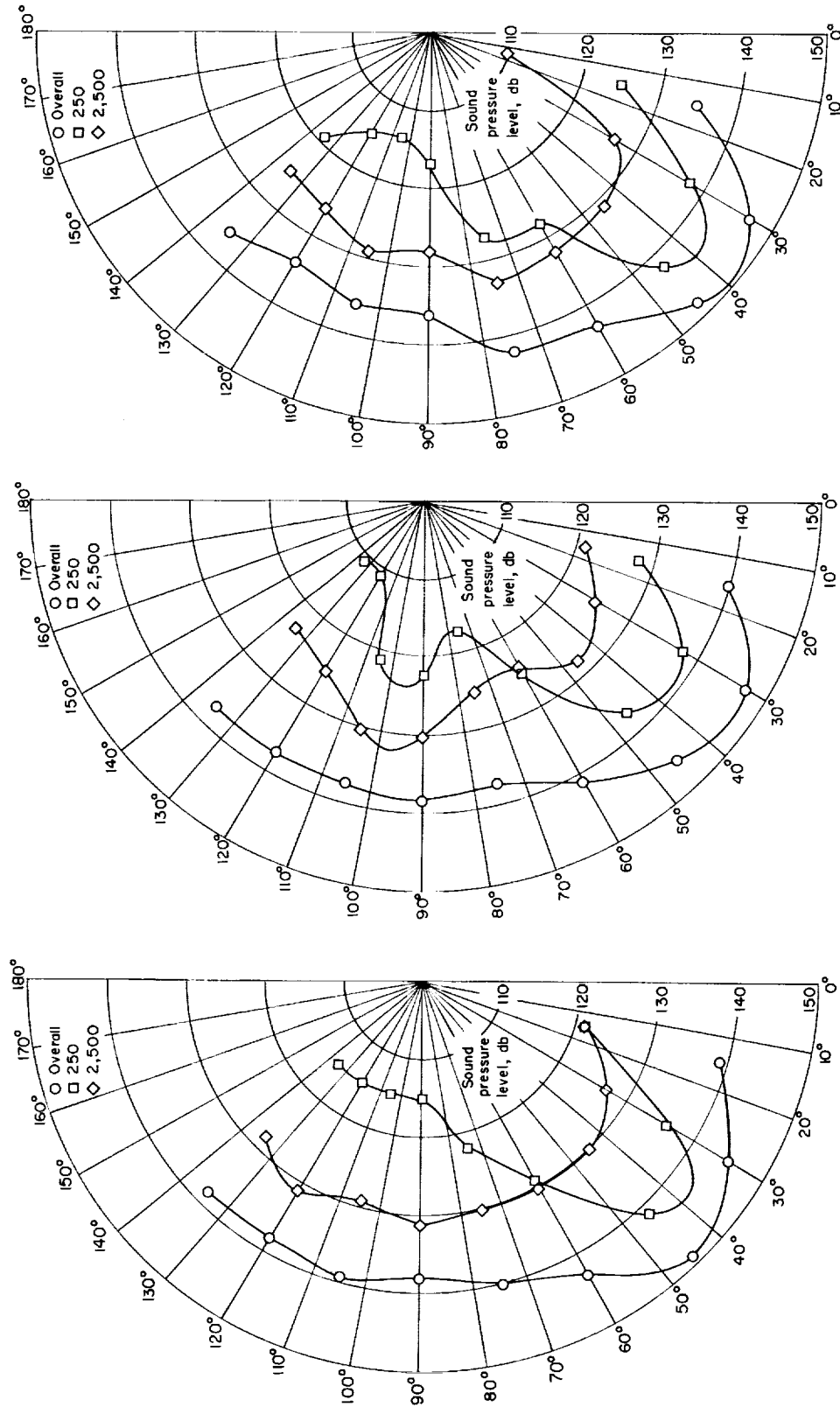
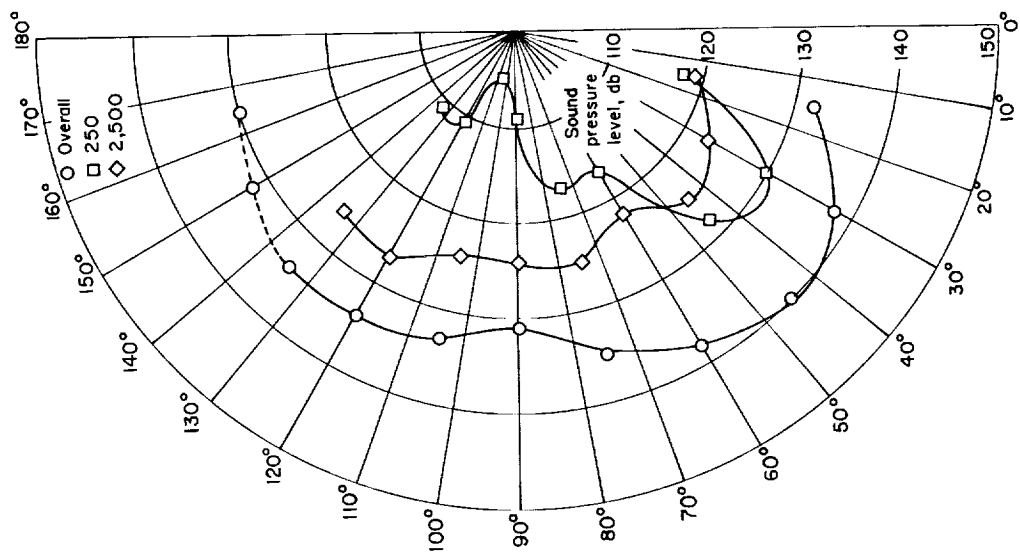
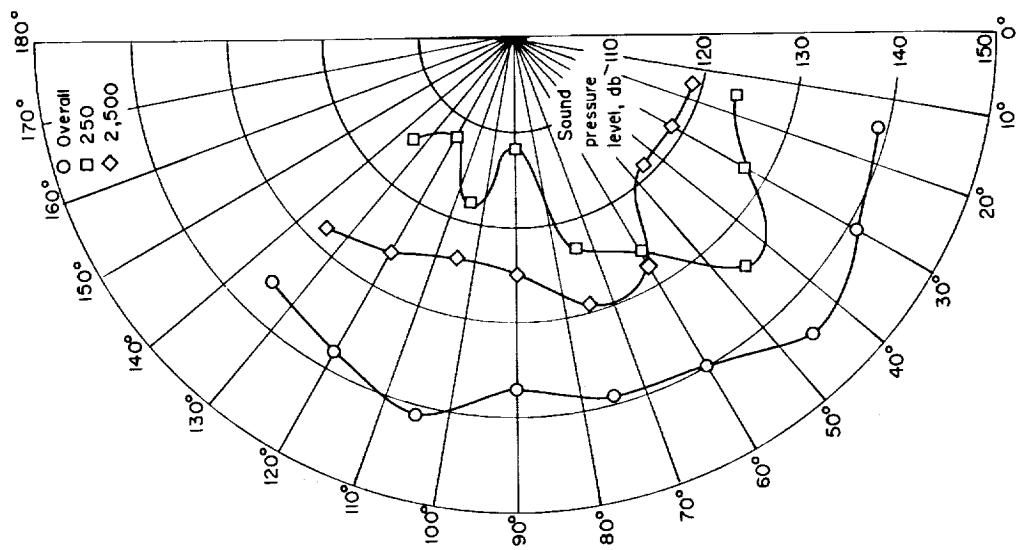


Figure 11.- Polar diagrams of sound pressure levels in three frequency bands for several rocket engines. Sound pressure levels measured at a radius of 50 feet.



(e) Engine F.



(d) Engine F.

Figure 11.- Concluded.

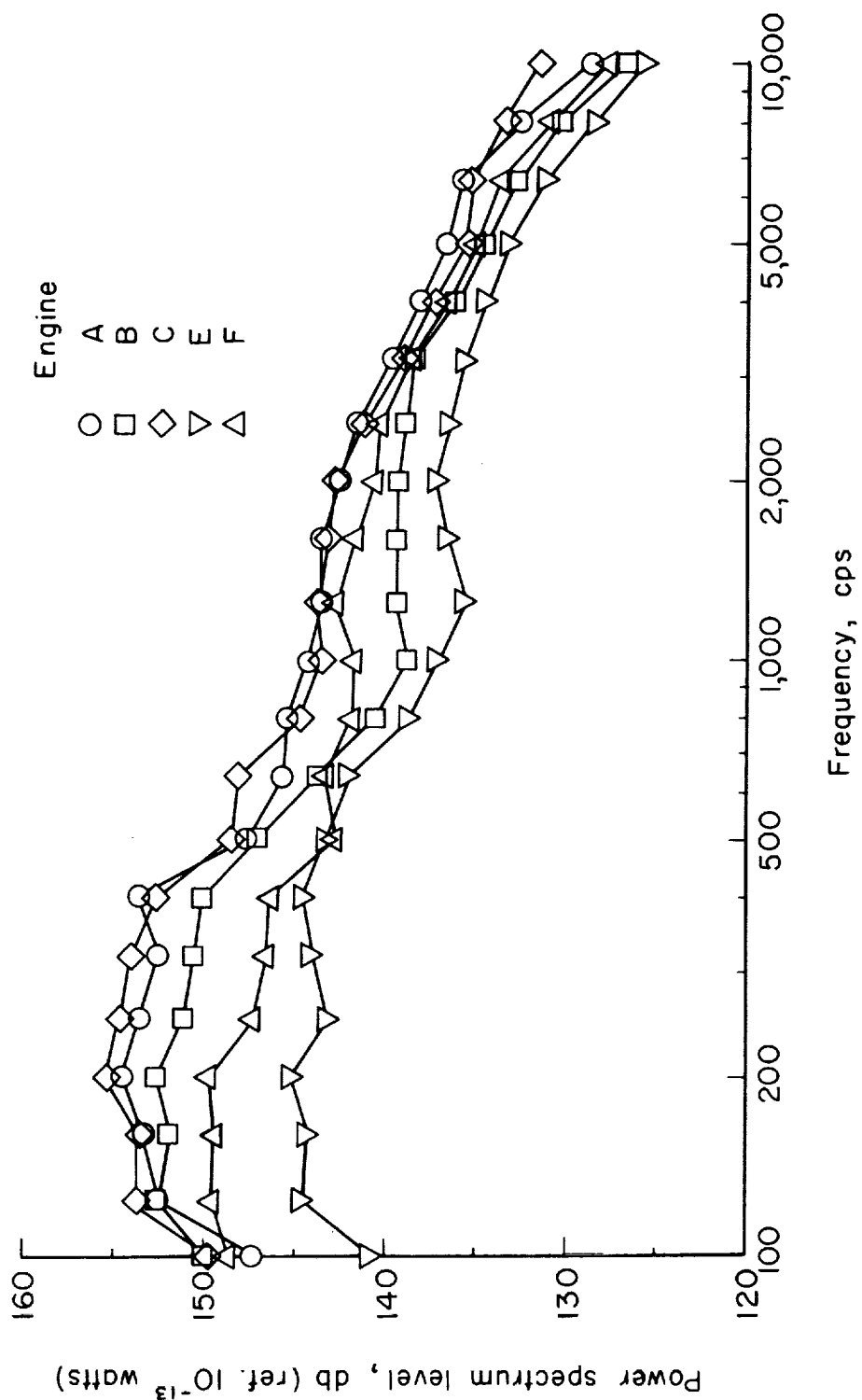


Figure 12.- Power spectrum level in decibels as a function of frequency for five rocket engines.

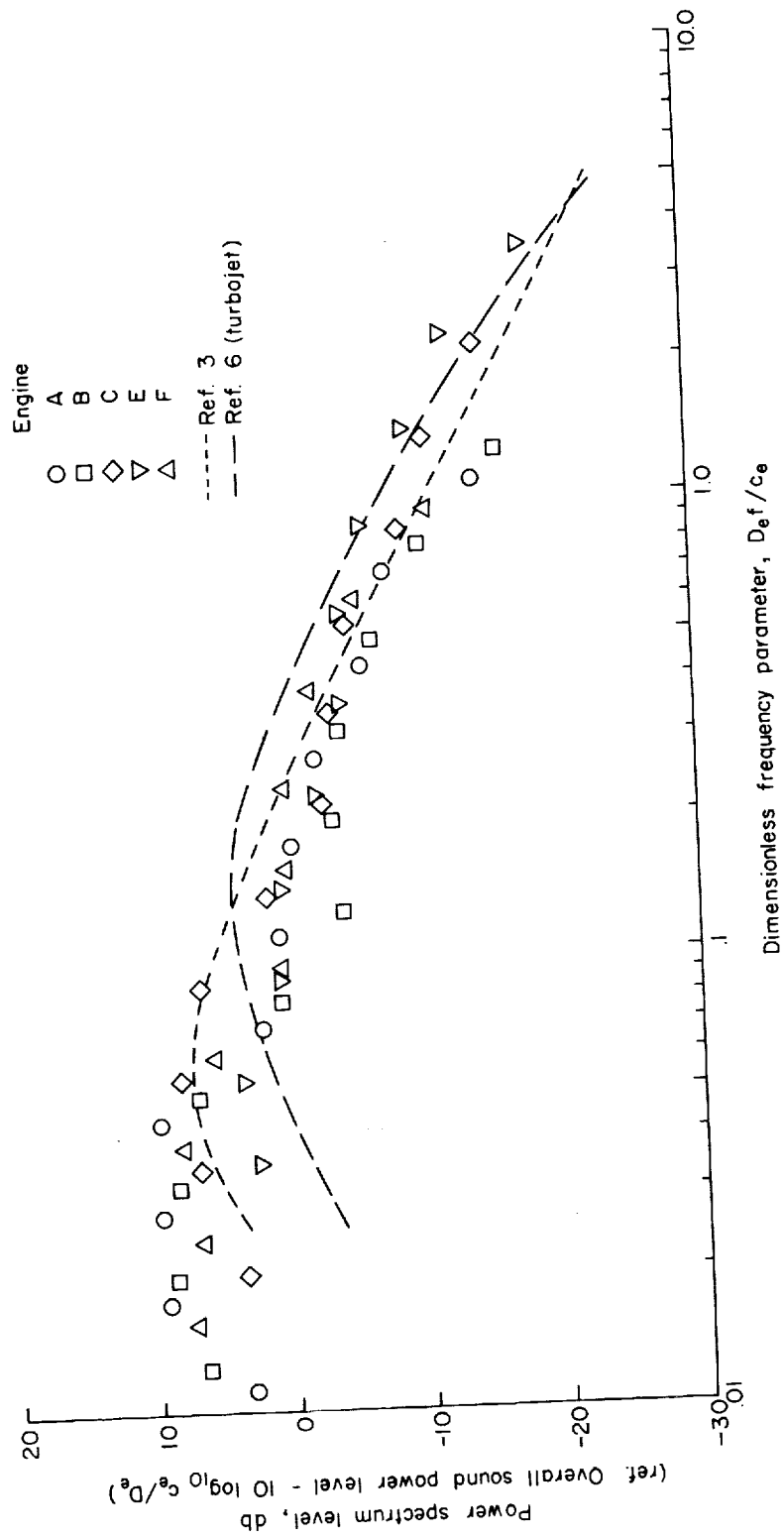


Figure 13.- Generalized power spectrum of rocket noise.

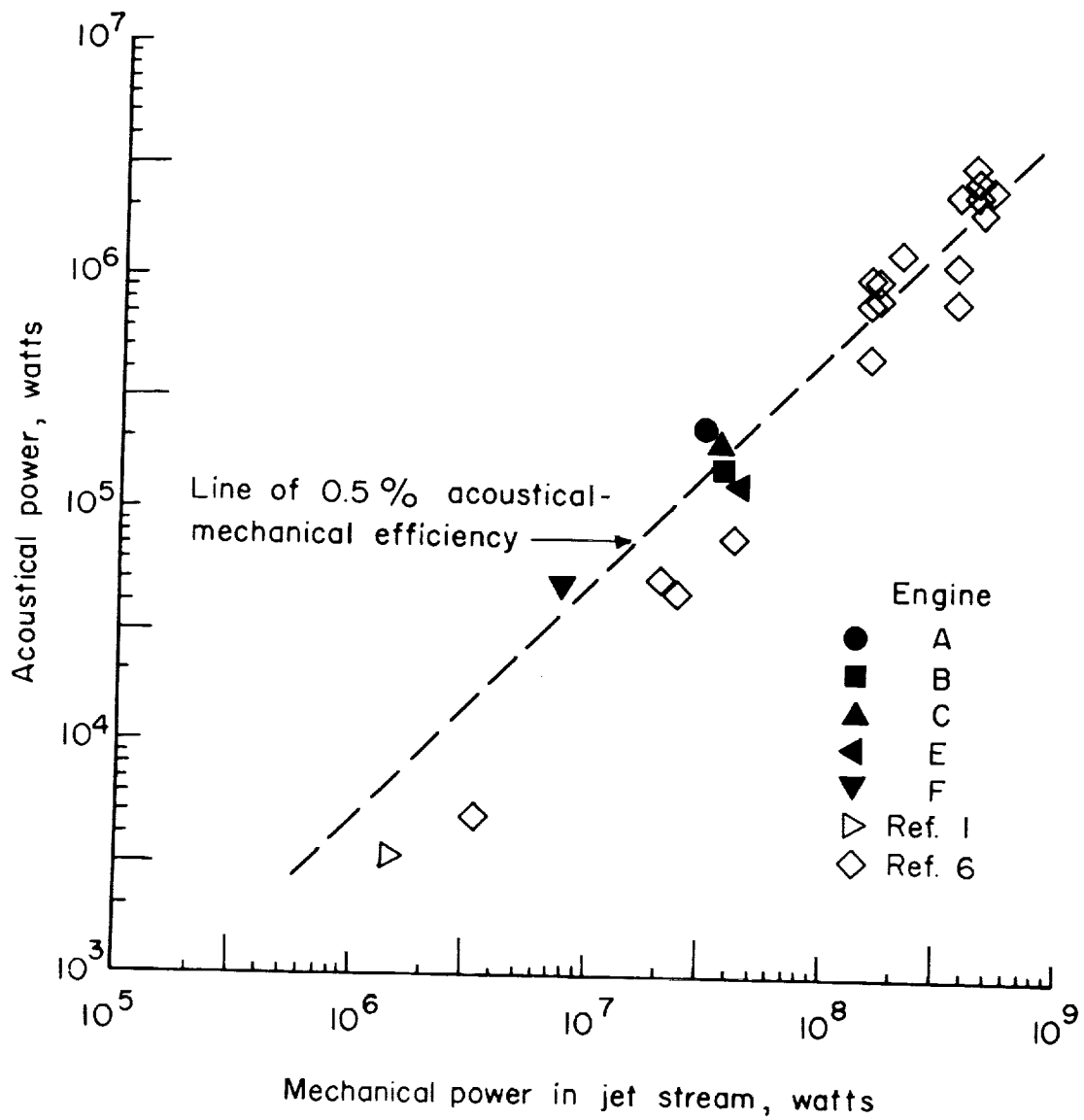


Figure 14.- Total acoustical power radiated by several rocket engines as a function of mechanical power in the jet stream.